

Kinematics of foraging dives and lunge-feeding in fin whales

Jeremy A. Goldbogen^{1,2,*}, John Calambokidis³, Robert E. Shadwick¹, Erin M. Oleson²,
 Mark A. McDonald⁴ and John A. Hildebrand²

¹Department of Zoology, University of British Columbia, 6270 University Boulevard, Vancouver, British Columbia, V6T 1Z4, Canada, ²Scripps Institution of Oceanography, University of California, San Diego, La Jolla, CA 92093-0205, USA, ³Cascadia Research Collective, Olympia, WA 98501, USA and ⁴Whale Acoustics, Bellvue, CO 80512, USA

*Author for correspondence (e-mail: jergold@zoology.ubc.ca)

Accepted 31 January 2006

Summary

Fin whales are among the largest predators on earth, yet little is known about their foraging behavior at depth. These whales obtain their prey by lunge-feeding, an extraordinary biomechanical event where large amounts of water and prey are engulfed and filtered. This process entails a high energetic cost that effectively decreases dive duration and increases post-dive recovery time. To examine the body mechanics of fin whales during foraging dives we attached high-resolution digital tags, equipped with a hydrophone, a depth gauge and a dual-axis accelerometer, to the backs of surfacing fin whales in the Southern California Bight. Body pitch and roll were estimated by changes in static gravitational acceleration detected by orthogonal axes of the accelerometer, while higher frequency, smaller amplitude oscillations in the accelerometer signals were interpreted as bouts of active

fluking. Instantaneous velocity of the whale was determined from the magnitude of turbulent flow noise measured by the hydrophone and confirmed by kinematic analysis. Fin whales employed gliding gaits during descent, executed a series of lunges at depth and ascended to the surface by steady fluking. Our examination of body kinematics at depth reveals variable lunge-feeding behavior in the context of distinct kinematic modes, which exhibit temporal coordination of rotational torques with translational accelerations. Maximum swimming speeds during lunges match previous estimates of the flow-induced pressure needed to completely expand the buccal cavity during feeding.

Key words: fin whale, *Balaenoptera physalus*, diving, lunge-feeding, swimming, kinematics.

Introduction

Marine mammals face the challenge of performing energetic tasks while breath holding (Butler and Jones, 1997; Kooyman and Ponganis, 1998). Conflicting metabolic demands of locomotor activity with a limited oxygen supply must therefore be balanced in order to maximize foraging efforts at depth (Castellini et al., 1985; Hochachka, 1986; Davis et al., 2004). Limits to diving capacity, defined by the ability to aerobically dive deeper and longer, are determined by the magnitude of oxygen stores within the body and the rate at which that oxygen supply is consumed (Scholander, 1940; Snyder, 1983; Kooyman, 1989). As body size increases, oxygen stores increase while mass-specific metabolic rates decrease (Klieber, 1932), suggesting that larger animals should be able to dive longer (Butler and Jones, 1982). In general, marine mammals have indeed been shown to dive longer and deeper with increasing size, although this allometric relationship appears to be effected by ecological, behavioral and physiological differences among species (Shreer and Kovacs, 1997; Noren and Williams, 2000; Halsey et al., 2006). Ultimately, oxygen

stores must be used wisely during a dive through the implementation of strategies to reduce the cost of locomotion.

Cetaceans and phocid seals use lift to generate thrust by the periodic oscillation of a crescent-shaped hydrofoil (Fish et al., 1988; Fish, 1993b; Fish, 1998; Fish and Rohr, 1999). The number of strokes taken during a dive directly increases the energetic cost of foraging (Davis et al., 1985; Fish et al., 1988; Williams et al., 2004). To reduce this cost and enhance diving capacity, locomotor activity is decreased by taking advantage of changes in buoyancy associated with lunge collapse at depth and employing gliding or stroke-and-glide gaits (Skrovan et al., 1999; Williams et al., 2000; Williams, 2001). Differences in body composition among different marine mammals permit the use of gliding gaits at different stages of a dive. Phocid seals (Sato et al., 2003), bottlenose dolphins (Skrovan et al., 1999) and blue whales (Williams et al., 2000) glide during descent and actively stroke to the surface, whereas more positively buoyant right whales (Nowacek et al., 2001) and sperm whales (Miller et al., 2004) actively stroke to depth and glide more during ascent. Drag forces resist forward motion of the body throughout

a dive and pose a considerable energetic cost, but the fusiform body shape characteristic of all accomplished swimmers reduces drag by minimizing the development of pressure gradients along the body and delaying separation of a turbulent boundary layer (Vogel, 1994; Fish, 1993a; Fish and Rohr, 1999).

The fin whale, *Balaenoptera physalus* (Linnaeus 1758), is a fast, streamlined swimmer and one of the largest animals on earth (Bose and Lien, 1989; Bose et al., 1990). Mysticete cetaceans of the crown group Balaenopteridae (*sensu* Rice, 1998), namely blue and fin whales, exhibit significantly shorter dive durations than would be predicted from their extreme body size (Croll et al., 2001). The rorquals are most notably distinguished from other baleen whales by their lunge-feeding behavior, an extraordinary biomechanical process in which large amounts of water and prey are engulfed and filtered (Brodie, 1993; Pivorunas, 1979; Werth, 2000). This mode of intermittent filter feeding requires that the whale uses inertia of the body to stretch its buccal cavity around a volume of prey-laden water (Orton and Brodie, 1987). Blue whale diving behavior combined with oceanographic data show that feeding efforts are primarily directed towards subsurface aggregations of euphausiid crustaceans associated with steep submarine canyon topography (Croll et al., 1998; Fiedler et al., 1998; Croll et al., 2005). Fin whale tracks are also closely linked to aggregations of krill and capelin situated against similar topographic features (Simard et al., 2002). Dive profiles of blue and fin whales reveal longer recovery time at the surface following foraging dives in comparison with non-foraging dives, suggesting that lunge-feeding is energetically costly and consequently limits maximum dive duration (Acevedo-Gutierrez et al., 2002).

Lunge-feeding is facilitated by a host of remarkable morphological and biomechanical adaptations, most of which have been described *post mortem*. The throat wall is lined with a series of longitudinal throat grooves that consist of tough ridges connected by furrows of delicate elastic tissue (Brodie, 1977; Orton and Brodie, 1987; deBakker et al., 1997). The ventral groove blubber is reversibly extensible up to several times its resting length to accommodate an expanding buccal cavity during engulfment feeding (Orton and Brodie, 1987). From the forces required to stretch this tissue, Orton and Brodie predicted that a swimming speed of 3.0 m s^{-1} would generate enough hydrodynamic force to completely inflate the buccal cavity (Orton and Brodie, 1987). Opening of the mouth causes a lateral expansion and outward rotation of the mandibles, effectively increasing surface area of the mouth to oncoming flow (Lambersten et al., 1995). Excellent underwater video footage of lunging dwarf minke whales has confirmed this phenomenon of mandible rotation *in situ* (Arnold et al., 2005). An elastic, weakly muscularized tongue is thought to initiate distension of the ventral pouch and increase the capacity of the mouth through invagination into a hollow sac (Lambertsen, 1983). A well-developed coronoid process of the mandible is mechanically linked to the frontal bone by a fibrous frontomandibular stay that is closely associated with the temporalis muscle (Lambersten et al., 1995). This tendon may

act to limit hyperdepression of the lower jaw, provide elastic recoil to reverse the direction of jaw movement, and enhance mechanical power output of the temporalis when acting to elevate the lower jaw (Lambersten et al., 1995). Once the jaws have closed around the volume of prey-laden seawater, a novel articulation between the mandibles and maxillary suborbital plate may provide a hydrodynamic seal of the buccal cavity, thereby maintaining a fusiform body shape in spite of possessing a highly expandable mouth (Lambertsen and Hintz, 2004). The forces to deflate the ventral pouch are suggested to come from the dynamic pressure from oncoming flow, elastic energy stored within the stretched tissues and active muscle shortening beneath the blubber (Orton and Brodie, 1987). Video footage at the sea surface of lunge-feeding rorquals has provided evidence of a rebounding wave within the ventral pouch that is thought to enhance filtration (Kot, 2005).

Our knowledge of the lunge-feeding process *in situ* is limited to aerial or ship observations near the sea surface. Humpback whales lunge-feeding at the sea surface exhibit three kinematic modes that are distinguished by the orientation of the body with respect to the water surface (Jurasz and Jurasz, 1979). Two of these modes were termed 'lateral lunge feeding' and 'inverted lunge feeding', which involved rotations about the whale's longitudinal axis (roll) of approximately 90° and 180° , respectively (Jurasz and Jurasz, 1979). Lateral lunge-feeding was also observed for blue and fin whales surface-feeding on euphausiids or schooling fish (Andrews, 1909; Tomilin, 1957; Watkins and Schevill, 1979; Gaskin, 1982; Corkeron, 1999). However, Watkins and Schevill reported that fin whales primarily lunged with their ventral sides down (Watkins and Schevill, 1979). Underwater observations of lunge-feeding include humpbacks executing lateral lunges while bottom feeding on sand lance at 30 m depth (Hain et al., 1995) and Crittercam video of a blue whale performing inverted lunges on pelagic krill aggregations (J.C., personal communication). Fin whales have also been observed to feed in shallow waters on sand lance (Bigelow and Schroeder, 1953; Overholtz and Nicolas, 1979) and herring (Nottestad et al., 2002), but the types of feeding modes used were not reported. Overall, lunge-feeding behavior appears to be modal as well as highly variable across species, but the detailed mechanics of the process remain elusive.

To investigate the swimming kinematics during foraging dives, we attached high-resolution digital tags to the backs of surfacing fin whales in the Southern California Bight. Accelerometer data were used to analyze both body orientation and fluking behavior, while hydrophone-measured flow noise was used to estimate body speeds throughout the dive cycle. We present the first kinematic analysis of a diving rorqual, including lunge-feeding behavior at depth.

Materials and methods

Digital tag

The high-resolution digital tag (Bioacoustic Probe; Greeneridge Sciences, Inc., Goleta, CA, USA; Burgess et al.,

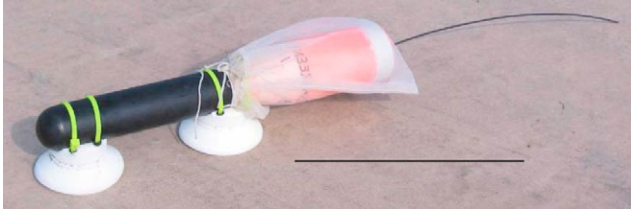


Fig. 1. Bioacoustic probe. The high-resolution digital tag contains a depth gauge, a two-axis accelerometer and a hydrophone (Bioacoustic Probe; Burgess et al., 1998). The tag was harnessed with silicon suction cups for attachment and a flotation device for retrieval. Scale bar, 20 cm.

1998) included a hydrophone (sampling rate, 1025 Hz), a depth gauge and a two-axis accelerometer (MXA2500GL/ML; MEMSIC Inc., North Andover, MA, USA) encapsulated in a cylindrical polyurethane shell with a hemispheric nose. Data from the depth gauge and accelerometer were digitally recorded at 1 Hz and stored within the tag. The tag was attached to two silicon suction cups with zip-ties and harnessed with a flotation device (Fig. 1). Typically, the tag stayed attached for several hours, fell off during lunges at depth and then floated to the surface. Upon tag recapture, the data were downloaded for analysis *via* infrared transmission.

Tagging methodology

Fin whales (*Balaenoptera physalus*; family Balaenopteridae) were tagged off the Tanner-Cortez banks in the Southern California Bight during a visual and acoustic marine mammal monitoring operation in the summer of 2003 (Oleson, 2005). A 5.3 m Rigid-Hulled Inflatable Boat approached whales from behind, and tags were attached using a 4 m fiberglass pole. We aimed to place the tag so that its long axis was largely parallel with the long axis of the animal (Fig. 2). However, as soon as the whale started to dive, it was apparent that flow forces helped to align the tag more parallel with the longitudinal axis of the body. When possible, tagged whales were followed visually or by radio VHF transmission.

Whale speed estimates

Flow noise has previously been used as a method for estimating flow speed (Finger et al., 1979; Fletcher et al., 1996; Burgess et al., 1998). We utilized this approach to estimate the instantaneous speed of whales for a given level of flow noise recorded by the hydrophone on the tag. To determine the magnitude of flow noise at different flow velocities, the tag was attached to a dihedral wing (V-FIN, Type 166; Endeco/YSI Inc., Marion, MA, USA) and towed at approximately 0, 1.5, 3.0 and 5.0 m s⁻¹ by the R/V *Sproul*. The flow noise was analyzed at different frequencies at each flow velocity by calculating the root-mean-square sound pressure over 1/3 octave bands. The 50 Hz spectrum exhibited both the highest flow noise level and the most distinct partitioning of this noise level for each flow velocity. Therefore, we used the 50-Hz 1/3 octave band of the flow noise signal in order to determine flow



Fig. 2. A tagged fin whale, showing placement of the bioacoustic probe during surfacing. Superimposed onto the image are the orthogonal axes of the accelerometer. The long axis of the tag was largely parallel with the longitudinal axis of the animal on all successful deployments. The x -axis is parallel with the long axis of the tag (red) and the y -axis extends radially on the tag (blue). Each axis detects static acceleration (A_x , A_y) in order to estimate the orientation of the animal in dimensions as defined by rotation about the y -axis, pitch (γ), and about the x -axis, roll (θ). An axis oriented parallel to gravity would result in 1.0 g recorded by the accelerometer, whereas an axis perpendicular to gravity would produce a 0.0 g accelerometer signal. Small-scale, dynamic oscillations detected by the x -axis were interpreted as fluking. The R/P *FLIP*, visible on the horizon, served as a research platform for visual and acoustic marine mammal monitoring operations.

speed. A positive relationship between flow speed and flow noise was obtained through a least-squares curvilinear regression (Fig. 3; $r^2=0.99$). This relationship was used to calculate instantaneous velocity, V_S , for a given flow noise level recorded from the tag deployments. As a corollary, whale speed derived from the kinematics of the body, V_K , was estimated by dividing the vertical velocity obtained from the depth profile by the sine of the body pitch angle (see Miller et al., 2004). The first derivative of speed with respect to time was determined in order to estimate the instantaneous acceleration of the body throughout the dive cycle.

Body orientation: theory

The accelerometer measured both static (gravitational acceleration) and dynamic acceleration at 1 Hz, which allowed for the analysis of body orientation and fluking, respectively. Accelerometer signals were low-pass filtered (cutoff frequency, 0.1 Hz) to remove higher frequency oscillations for analysis; the low-frequency signal became the data used to determine orientation while the high-frequency signal was used to analyze fluking patterns (see Fluking analysis section below). A linear scaling adjustment performed at acquisition time accounted for the fact that the accelerometer was being sampled before it completely settled (W. C. Burgess, personal communication).

Body orientation was represented by two kinematic degrees of freedom: pitch and roll. The x -axis was defined as the long

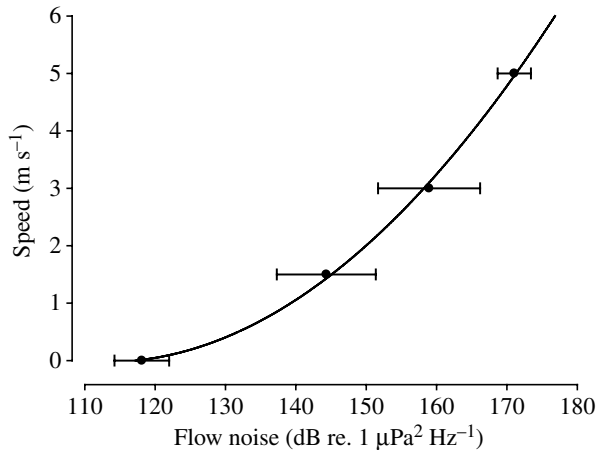


Fig. 3. Flow noise increases with flow speed. The tag was attached to a wing and towed at different speeds in order to establish a relationship between flow noise magnitude and flow velocity. Flow noise was determined by calculating the root-mean-square sound pressure at the 50-Hz 1/3 octave bands. The 50-Hz 1/3 octave band was chosen because it exhibited both a high flow noise level and a distinct partitioning of flow noise magnitude for each flow velocity. The least-squares regression through the data is described by the equation $y=0.0015x^2-0.3327x+18.748$; $r^2=0.99$. This equation was used to estimate the instantaneous speed of the whale throughout the dive cycle for a given level of flow noise recorded by the tag.

axis of the tag, which is parallel to one axis of the accelerometer, while the y -axis was defined as perpendicular to this axis, which extends radially on the tag. Acceleration along each axis was measured in gravitational units (range, $\pm 1 g$; $g=9.8 \text{ m s}^{-2}$). Changes in acceleration detected by the x -axis were used to estimate body pitch or tilt:

$$\gamma = \text{asin}(A_x/A_x^*), \quad (1)$$

where A_x is the static acceleration measured along the x -axis of the accelerometer, A_x^* is the maximum value recorded by the accelerometer along that axis ($1.0 g$), and γ is the pitch of the long axis of the animal with respect to horizontal. Equation 1 describes the revolution of the accelerometer axis about the arc of a unit circle and its resulting nonlinear response. Therefore, $\gamma=0^\circ$ would represent a horizontal body angle and $\gamma=\pm 90^\circ$ would reflect vertical body orientations.

Rotations about the x -axis signify body roll and will be observed in changes in static acceleration by the y -axis of the accelerometer, A_y . Body roll estimates are affected by different pitch orientations such that progressive degrees of tilt significantly decrease the magnitude of static acceleration measured along the y -axis. Instead of the accelerometer axis revolving about the arc of a circle, its path effectively becomes an arc of a projected ellipse of diminished height onto the plane perpendicular to gravity. The magnitude of reduced height of the projected ellipse is determined by:

$$\hat{h} = \cos(\gamma). \quad (2)$$

Substituting \hat{h} into the equation for an ellipse and keeping the

other axis of the ellipse perpendicular to gravity (width) equivalent to a unit circle, the angle of revolution, θ , about this ellipse is augmented to become:

$$\theta = \left[\frac{1}{1 - \left(\frac{A_x}{A_x^*} \right)} \right] \left[\cos(\text{asin } A_x) \right]^2 \left[\text{asin} \left(\frac{A_y}{A_y^*} \right) \right], \quad (3)$$

where A_y^* is the maximum value recorded by the accelerometer when the y -axis is parallel to gravity.

The three terms of Eqn 3, as denoted by brackets, each describe a particular characteristic of the accelerometer response, which ultimately combine to give a roll estimate, θ , for a given output of the dual axis accelerometer within the tag. Term 1 describes a 'tilt factor', where high levels of pitch drastically increase the sensitivity of the response and decrease the overall magnitude of the response. Term 2 is related to an ellipse of decreasing height with increasing values of body pitch, while term 3 is analogous to Eqn 1, the revolution about an arc of a unit circle.

Body orientation: calibration

To experimentally test the validity of Eqn 3, the accelerometer was calibrated in a custom-made device. The apparatus statically held the tag at different degrees of tilt. At each level of tilt, as determined by Eqn 1, the tag was rolled at 5° intervals as measured by a laser pointer and protractor attached parallel to the long axis of the tag. Data from this calibration were used to describe the range of θ in the context of the orthogonal dependence of A_y on A_x (Fig. 4). For static orientations, the maximum value recorded by the accelerometer was $0.9 g$, which may be due to the interaction between sampling and settling rates of the accelerometer (W. C. Burgess, personal communication). However, standardizing the response with respect to the maximum value is expected to account for this difference (Eqns 1, 3).

The accelerometer data from the static calibration (Fig. 4) were entered into Eqn 3 to determine what roll angle would be predicted by theory. Roll angles predicted by theory compared with the roll angles measured experimentally showed a strong correlation (Fig. 5; $r^2=0.99$), suggesting that Eqn 3 is a reliable method to estimate body roll at pitch angles less than 65° . At the highest degrees of roll, when the y -axis of the accelerometer is nearly parallel to gravity, we suggest a maximum error of approximately $\pm 10^\circ$. At low to moderate pitch and roll angles we expect error to be less than $\pm 5^\circ$.

The range of θ is limited to 180° if the axis of the accelerometer begins in the plane parallel to gravity, whereas the range of θ is limited to 90° if the axis begins in the plane perpendicular to gravity. This dependence of A_y on A_x did not allow for an analysis of roll angle during descent or ascent where γ exceeded 65° and high A_x values were involved.

The position of the tag may move during the course of the dive, which would significantly alter kinematic analysis. To

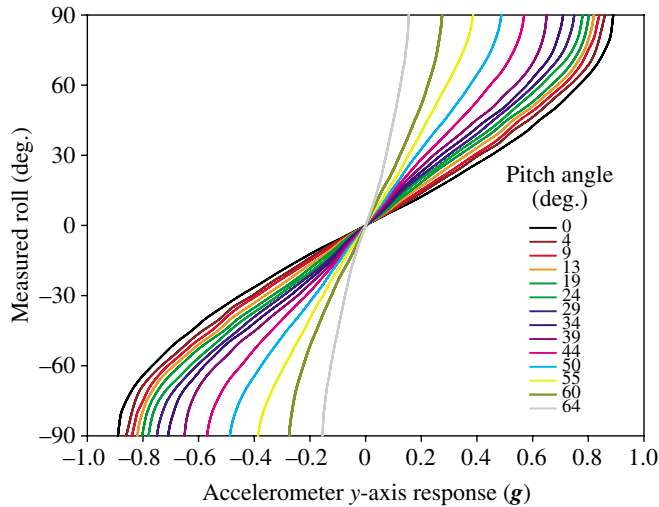


Fig. 4. Dual-axis accelerometer response as a function of pitch angle. The tag was held statically at different pitch angles and rolled at 5° intervals. Data points represent mean static acceleration measured by the y-axis (A_y) of the accelerometer from three different tags. Varying pitch angles are characterized by different colors as defined in the legend. At high pitch angles, the magnitude of the accelerometer response decreases along the y-axis.

address this potentially confounding factor, tag orientation was examined when the whale was at the surface. Before and after each dive, the mean pitch angle was $2.5 \pm 2.7^\circ$ ($N=28$) from horizontal when the whale was at the surface, suggesting that the tag was largely parallel with the long axis of the whale's body and maintained this orientation throughout the deployment. The orientation of the y-axis of the accelerometer (radial axis of the tag) was also determined before and after a dive. In this way, sliding of the tag was sometimes observed, which discounted the dive from being included in further analysis. With the assumption that the whale did not roll on average while at the surface, the average value of A_y was recorded at the surface. This served as an indication of when the whale was level at depth and also to what extent the body rolled during lunges or maneuvers.

Fluking analysis

Dorsal–ventral oscillations of the flukes were detected as small-amplitude oscillations by the x-axis of the accelerometer. These distinct patterns of dynamic acceleration, likely to be a result of recoil forces manifest throughout the body (see Fish et al., 2003), were isolated from the static acceleration profile used to determine body orientation by low-pass filtering at 0.10 Hz. These patterns were so distinct and repeatable in form and fashion that we consider this filtering process to have removed all accelerations due to fluking itself. However, it was not possible to account for surge, heave or sideslip (see fig. 8 in Fish, 2004 for definitions) that may have contributed to the accelerometer signal. Fluking frequencies were calculated by counting the number of acceleration maxima divided by the

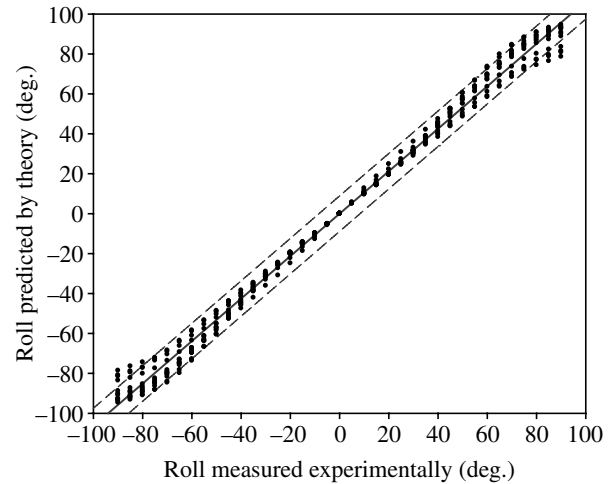


Fig. 5. Roll predicted by theory (see Eqn 3) accurately predicts roll measured experimentally by static calibration. The solid line represents the least-squares linear regression through the data ($r^2=0.99$). The broken lines mark 95% prediction intervals.

time of a given bout of fluking. Either through recoil forces detected by the tag in the mid-body region or by actual tilting with the caudal stock, downstrokes produced positive peaks in the fluking profile while upstrokes resulted in negative peaks.

Dive profiles

Data from the pressure transducer within the tag recorded changes in depth over time and provided a context for which to evaluate other kinematic parameters. Depth profiles were categorized into several phases. Descent was defined as the time between a depth value of zero and the time when maximum velocity was recorded, since each whale continued to accelerate until a preferred depth was attained. Ascent time was defined as the time from the last velocity minimum (end of last lunge) until the time when depth equaled zero again. Lunging time, or foraging time, was defined as the time between descent and ascent. Post-dive time, or recovery time, was the time spent at the surface after a dive, until another foraging dive was recorded.

A series of vertical excursions at the bottom of a dive was assumed to represent a foraging dive. Although we have no direct video evidence to confirm that these whales were actually feeding, previous studies have shown that these vertical excursions occur at the precise location of their preferred prey (Croll et al., 1998; Croll et al., 2005). Crittercam deployments on blue whales also confirm the presence of prey during these types of lunges.

Statistics

All statistical analyses were performed using Minitab (version 13). If a parameter failed, the Anderson–Darling test for normality, a Mann–Whitney U -test, was used to test whether two given kinematic parameters were significantly different from one another. A P -value less than or equal to 0.05

Table 1. Dive data summary for tagged fin whales

Whale	Date	Number of dives	Dive duration (min)	Maximum dive depth (m)	Descent duration (min)	Maximum descent		Mean descent angle (deg.)	Proportion of descent gliding (%)	Number of lunges per dive	Ascent duration (min)	Maximum ascent		Mean ascent angle (deg.)	Ascent fluking frequencies (Hz)
						speed (m s ⁻¹)	speed (m s ⁻¹)					speed (m s ⁻¹)	speed (m s ⁻¹)		
A	20 Aug 03	8	7.3±0.6	228±9	1.7±0.4	5.8±0.3	3.4±0.2	-57±9	37±14	3.5±0.5	1.3±0.3	3.6±0.5	2.2±0.3	60±7	0.29±0.02
B	21 Aug 03	1	7.9	267	2.0	5.6	3.7	-57	43	6	1.3	4.0	2.5	70	0.23
C	22 Aug 03	6	7.2±0.4	257±4	1.9±0.1	5.7±0.1	4.0±0.3	-48±4	69±18	5.5±0.8	1.4±0.2	3.3±0.3	2.4±0.4	65±6	0.30±0.02
D	23 Aug 03	1	6.9	238	2.3	5.4	3.5	-61	31	4	1.3	2.6	2.1	47	0.27
E	25 Aug 03	6	6.2±1.1	242±14	1.6±0.4	5.7±0.3	3.9±0.3	-48±9	74±14	3.8±1.9	1.7±0.3	3.2±0.3	2.4±0.2	65±4	0.31±0.01
F	26 Aug 03	5	6.2±0.5	270±4	1.6±0.3	5.9±0.1	3.9±0.6	-55±7	54±28	4.4±1.7	1.4±0.4	3.6±0.2	2.4±0.2	67±6	0.30±0.01
G	26 Aug 03	1	8.0	271	2.0	5.1	3.3	-52	44	6	1.8	3.5	2.6	64	0.21
Overall mean			7.0±1.0	248±18	1.7±0.4	5.7±0.3	3.7±0.4	-53±8	55±23	4.4±1.4	1.4±0.3	3.4±0.4	2.4±0.3	64±7	0.29±0.03

Values are means ± s.d.

accepted the hypothesis that the two parameters were significantly different. Sample sizes among individuals did not allow for an effect of individuals to be assessed.

Results

From 13 total attempts, seven fin whales were successfully tagged from 20 to 26 August 2003, resulting in 28 foraging dives recorded for analysis (Table 1). All tagged whales would consistently dive to depths below 200 m, making a concerted effort to dive to a preferred depth where lunges took place and ascend back to the sea surface. Maximum depth attained during each dive in the context of local bathymetry suggests that foraging occurred very close to the sea floor. All feces seen from these fin whales were composed of euphausiids. However, there may have been a bias since feces composed of fish is sometimes darker and more difficult to notice. Dive durations averaged 7.0±1.0 min (minimum, 4.6 min; maximum, 8.2 min) and were responsible for approximately 60% of each whale's total time budget, while the other 40% of the time the whales were closely associated with the sea surface (depth <50 m).

Kinematics during descent and ascent

A representative foraging dive recorded by the tag is presented in Fig. 6. At the beginning of descent strong fluking was observed, but stopped or decreased dramatically (<0.1 g) at a depth of 21±7 m. At the end of descent, small amplitude oscillations (<0.1 g) were often observed in the fluking profile, but we attributed these vibrations to an increasingly turbulent flow regime associated with high speeds (>4 m s⁻¹). Prolonged gliding was employed during 55±23% of descent durations but ranged widely from 19 to 95%. Strong fluking was observed at the end of each descent. Stroke-and-glide gaits were sometimes observed for many whales on descent (Table 1). By contrast, steady fluking at a frequency of 0.30±0.03 Hz was observed on ascent of every dive recorded. At the end of each ascent, steady fluking discontinued at a depth of 30±5 m as whales glided to the surface.

The highest speeds of the body during the entire dive cycle were recorded on descent. A comparison of the two methods used to estimate speed shows striking similarity, particularly at speeds between 1 and 5 m s⁻¹ (Fig. 7). Since the calculation of V_K is extremely sensitive to low values of pitch, a comparison to V_S during ascent and descent was appropriate given that changes in pitch were minimal and far from zero. A least-squares linear regression through instantaneous speed values calculated *via* each method suggests that there is a one-to-one correlation between them ($N=4062$, $r^2=0.91$, $V_K=1.0024V_S+0.2013$). In this way, V_S was justifiably used as a method to estimate speed throughout the dive, particularly during lunges, where pitch values were close to zero, which would have resulted in spurious V_K estimates.

Whales continually accelerated throughout descent at an average pitch angle of -53±8° to a maximum speed of 5.7±0.3 m s⁻¹ (Fig. 6). As the bottom of the dive was reached,

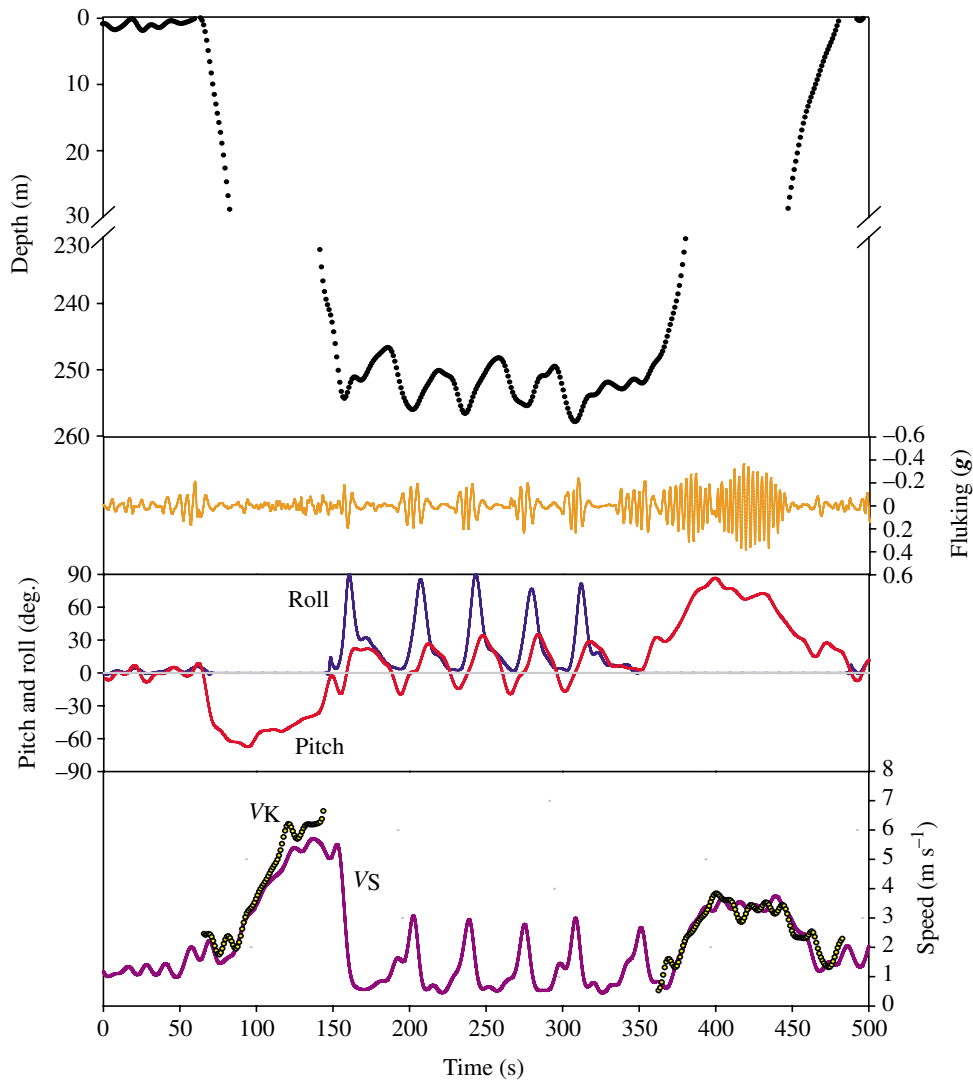


Fig. 6. A representative foraging dive, including five lunges at depth. Black dots correspond to depth over the course of the dive cycle. Fluking patterns are depicted by the orange line. Red and blue lines show changes of body pitch and roll, respectively. Instantaneous speed of the body estimated by flow noise (purple line) and from the kinematics of the body (yellow dots). Note that roll was not estimated during ascent and descent whereas instantaneous speed from the kinematics of the body was only calculated during these particular phases of the dive. Also note that there may be a lunge that occurs at the end of the initial descent.

Speeds during ascent were significantly lower and relatively more constant at steeper mean pitch angles of $64 \pm 7^\circ$ (Mann–Whitney U -test, $P < 0.005$), reaching maximum speeds of $3.4 \pm 0.4 \text{ m s}^{-1}$ (Table 1).

The relationship between body acceleration and body pitch during descent and ascent is shown in Fig. 8. At depths greater than 21 m on descent, where fluking had typically stopped, the body experienced net positive acceleration at relatively constant pitch angles, which indicated that

body speed decreased to very low speeds ($0.5\text{--}1.0 \text{ m s}^{-1}$) in approximately 5 s, representing a large deceleration, which perhaps indicated a lunge-feeding event upon initial descent.

the body was negatively buoyant and sinking. During ascent, body accelerations were much closer to zero, suggesting that a relatively constant speed was maintained, but gradually decreased as depth decreased. The highest decelerations were recorded at 30 m, the average depth at which gait transition from steady fluking to gliding took place.

Kinematics during lunges

A series of vertical excursions was typically observed at the bottom of each foraging dive that was associated with lunge-feeding behavior (Fig. 6). These excursions ranged from less than 5 m to as high as 20 m. Coincident with the depth

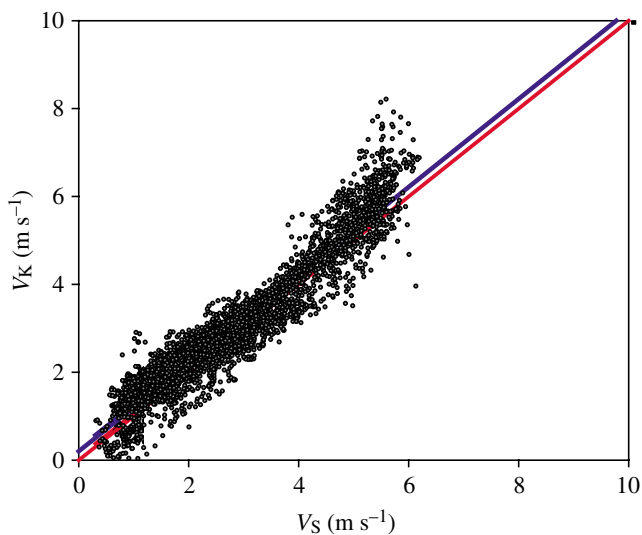


Fig. 7. Comparison of the two methods, V_S (flow noise) and V_K (kinematics), used to estimate speed of the body during descent and ascent (dark grey dots). The slope of the least-squares linear regression (blue line; $N=4062$, $r^2=0.91$, $P<0.001$) through all data points is not significantly different from unity (red line). Note that V_S tends to underestimate V_K at speeds greater than 5 m s^{-1} , the highest speed for which flow noise was recorded by the towed wing (Fig. 3).

minimum of each excursion was a distinct maximum in speed. We interpreted these speed maxima to represent lunge-feeding events; as the whale rushes toward a prey patch and opens its jaws, it will incur a massive drag load and decelerate rapidly. We arbitrarily defined a lunge to be a distinct speed maximum that is greater than 2.0 m s^{-1} . With this definition, we recorded 121 lunges during 28 foraging dives (Table 2). Whales executed anywhere from one to seven lunges per dive, but averaged 4.4 ± 1.4 per dive. Maximum speed during each lunge was $3.0 \pm 0.5 \text{ m s}^{-1}$ produced by fluking frequencies of $0.27 \pm 0.04 \text{ Hz}$. Speed values at one second intervals averaged from 50 lunges were calculated (1.26, 1.27, 1.29, 1.33, 1.44, 1.65, 1.93, 2.28, 2.64, 2.92, 3.03, 2.91, 2.56, 2.07, 1.57, 1.14, 0.85, 0.68, 0.60, 0.58, 0.61, 0.65, 0.69, 0.71, 0.70, 0.68 m s^{-1}). Whales glided until a bout of fluking marked another lunge-feeding event. Each bout of fluking lasted $16.2 \pm 3.9 \text{ s}$, while durations between consecutive lunges, the time between speed maxima, averaged $44.5 \pm 19.1 \text{ s}$ (Table 2).

A time series of fluking, body orientation, and translational acceleration during four consecutive lunges reveals a distinct and consistent kinematic mode (Fig. 9). Maxima, minima and zero values of each kinematic variable were superimposed onto depth profiles to determine the body dynamics that occur during a lunge. Before the lunge, the whale approaches a prey patch with a slight downward pitch ($\gamma < 30^\circ$). Maximum acceleration of the body typically occurred just as the first full stroke cycle was completed. At this moment the body begins to roll. The long axis of the body becomes level, parallel to the sea surface, as maximum velocity is reached. Opening of the mandibles, which is assumed to occur at maximum speed, causes a deceleration at the same time that the body completes a full 90° roll (Fig. 10). Meanwhile, the body begins to tilt upward and roll back as the final fluke stroke is executed. Maximum pitch is attained as the whale slows to a minimum speed.

This kinematic sequence was fundamentally conserved among all individuals, except for changes in body roll (Fig. 11). In these cases rolling was still observed, presumably a reflection of maneuvering, but the degree of roll was typically less than 45° and not temporally associated with other kinematic landmarks. Therefore, we categorized lunges into two modes based on the degree of roll and its temporal association with other kinematic parameters. Specifically, these modes were distinguished by the degree of roll observed at open gape, during maximum body deceleration. If the body was level, with its dorsal side facing the sea surface, the lunges were considered 'regular lunges' ($N=59$). The remaining lunges involved body rolls of $87 \pm 18^\circ$ ($N=62$) and were regarded as 'lateral lunges' (Table 2). Overall, lunge-feeding

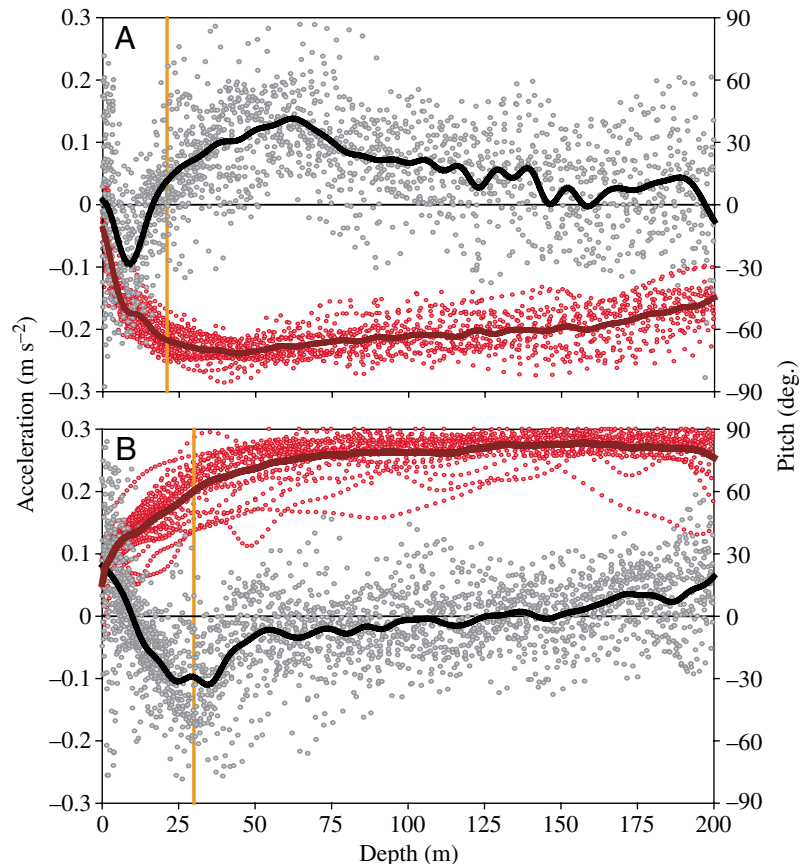


Fig. 8. Body acceleration (grey dots) and pitch (red dots) as a function of depth. Values are shown in the first 200 m of the water column and thus only show data for descent (A) and ascent (B). Positive acceleration is always in the direction of forward motion of the body. Thick lines represent the mean of each respective parameter at a particular depth. The orange vertical line denotes the mean depth where gait transition from fluking to gliding occurs during descent ($21 \pm 7 \text{ m}$, $N=28$) and during ascent ($30 \pm 5 \text{ m}$, $N=28$).

behavior was variable, with some individuals performing either lunge type exclusively and some exhibiting both kinematic modes, sometimes within the same dive.

Discussion

As the largest animals on earth, blue and fin whales face extraordinary consequences of an extreme body size (Calder, 1984). Mechanical principles predict that large body size will decrease agility and maneuverability (Webb and de Buffrenil, 1990). To circumvent these effects, balaenopterid foraging behavior incorporates the selection of dense aggregations of small prey (Weihs and Webb, 1983) and increased attacking speed during lunges (Fig. 9; Table 2). A large body size is accompanied by a high energetic demand such that *B. physalus* is predicted to require one metric ton of krill daily (Brodie, 1975). Physiological scaling laws suggest that increasing body size will increase oxygen stores and decrease mass-specific metabolic rate (Klieber, 1932). Thus, blue and fin whales appear well-equipped to aerobically dive longer and deeper to

exploit prey patches at depth. However, myoglobin concentration, the primary oxygen carrier in skeletal muscles, is relatively low for fin whales, indicating that rorquals have been subject to different selective pressures in terms of physiological adaptations to enhance dive capacity (Noren and Williams, 2000). Also, due to differences in body composition related to oxygen storage, cetaceans have considerably less oxygen per unit mass available compared with phocid seals and penguins (Kooyman, 1989).

Blue and fin whales typically dive much shorter (<17 min) and shallower (<200 m) than would be predicted by their large body size (Shreer and Kovacs, 1997; Croll et al., 2001). Although fin whales have been reported to dive as deep as 470 m, which is still somewhat shallow for their body size, dive durations during these excursions were less than 13 min (Panigada et al., 1999). Optimality models of dive behavior based on depth profiles of blue and fin whales suggest that lunge-feeding is energetically costly and thus responsible for limiting dive capacity (Acevedo-Gutierrez et al., 2002). Foraging dives in the Weddell seal are associated with an increased energetic cost compared with non-foraging dives of the same duration and such costs can be estimated from the number of strokes taken during a particular dive (Williams et al., 2004). Different types of locomotor activity, particularly involving rapid changes in translational and rotational acceleration, may significantly increase the energetic costs incurred during a dive (Weihs, 1981). While the energetic cost for each stroke does not change with body size among phocid seals (Williams et al., 2004), complex maneuvers executed by the largest whales may prove to be much more energetically expensive.

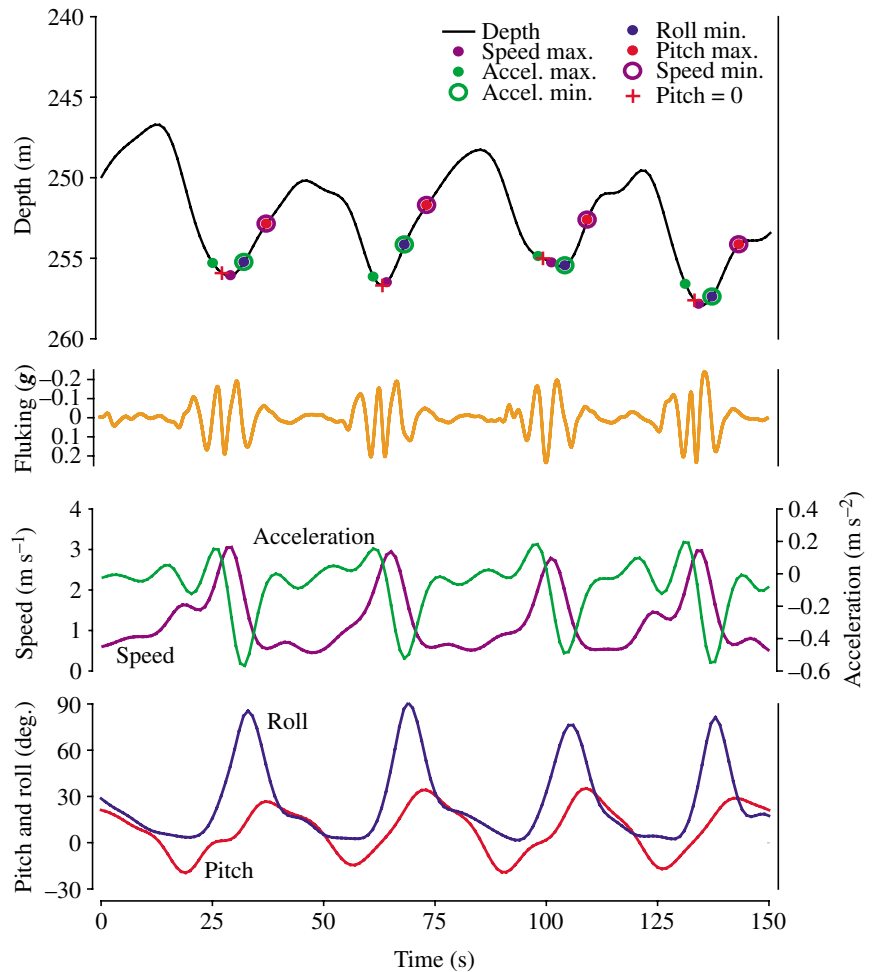
Here we show that fin whale foraging dives are characterized by a gliding descent, a series of lunges at depth and an ascent to the surface powered by steady fluking (Fig. 6). Other negatively buoyant marine mammals show similar patterns of reduced locomotor activity during descent (Skrovan et al., 1999; Sato et al., 2003), a behavior that is associated with a decrease in oxygen consumption, which in turn enhances diving capacity (Williams et al., 2000). Fin whales were observed to accelerate primarily while gliding at high descent angles (Fig. 8A), suggesting that buoyant forces are more effective when vertically directed drag forces are minimized. When the body is oriented more vertically, pressure drag is relatively lower because projected area is significantly decreased compared with when the body is broadside to vertically acting buoyant forces. In this way, whales accelerated to the highest velocities recorded over the dive cycle (Fig. 6). Similarly, sperm whales reached maximum speeds near the end of each descent, but such speeds were accompanied by fluking (Miller et al., 2004). Our data suggest that fin whales should be practically neutrally buoyant or slightly positively buoyant at depths shallower than 30 m, as indicated by the depth at which gait transition occurs during ascent and descent (Fig. 8; Table 1). This change in buoyancy is attributed to gradual lunge collapse with depth in other diving marine mammals (Skrovan, 1999;

Table 2. Lunge data summary for tagged fin whales

Whale	Number of lunges	Maximum speed (m s ⁻¹)	Lunge fluking frequency (Hz)	Lunge duration (s)	Time between consecutive lunges (s)	Change in pitch during lunge (deg.)	Change in roll during lunge (deg.)	Body pitch at jaw opening (deg.)	Lunge type
A	27	3.0±0.5	0.28±0.04	15±4	69±23	17±26	105±35	1±6	Ventral (21), Lateral (6)
B	6	4.0±0.2	0.28±0.02	14±2	43±6	44±9	89±3	8±5	Lateral
C	33	3.0±0.4	0.25±0.04	16±3	39±8	40±11	87±12	4±9	Lateral
D	4	3.0±0.3	0.27±0.07	15±1	41±9	42±10	85±7	-3±12	Lateral
E	23	2.5±0.4	0.28±0.03	16±3	33±8	-	-	-	Ventral
F	22	3.2±0.6	0.28±0.05	17±4	40±9	41±16	101±17	0±5	Ventral (9), lateral (13)
G	6	2.7±0.5	0.23±0.02	18±4	39±11	-	-	-	Ventral
Overall mean		3.0±0.5	0.27±0.04	16±3	45±19	39±15	87±18	3±8	

The last three parameters were only calculated for lateral lunges and are thus not shown for whales E and G. Values are means ± s.d. Number of observations for each lunge type is in parentheses.

Fig. 9. Detailed kinematics of the body and fluke during four consecutive lateral lunges at depth. The kinematic parameters presented over time include fluking dynamics (orange), acceleration (green) and speed (purple) of the body, and body pitch (red) and roll (blue). Fluking is derived from the small-scale, dynamic oscillations in the accelerometer signals. Dynamic acceleration values are presented with negative peaks pointing up and positive peaks pointing down to intuitively show upstrokes and downstrokes of the fluke, respectively (see Materials and methods for explanation). Instantaneous speed of the body is estimated from the magnitude of flow noise measured by the hydrophone. Body orientation is resolved in two dimensions from the changes in static acceleration along two orthogonal axes. Associated maxima (filled circles), minima (open circles) and zero values (crosses) of each kinematic parameter are superimposed onto the dive profile in the upper panel to illustrate the temporal coordination of rotational torques with translational accelerations. The onset of body acceleration and rotation are coincident with each fluking bout. The body becomes level prior to each lunge. Jaw opening is assumed to take place at maximum speed ($3.0 \pm 0.5 \text{ m s}^{-1}$; $N=62$; purple circles). Fluking continues after maximum velocity occurs. Maximum body deceleration and roll maxima ($87 \pm 18^\circ$; $N=62$) occur concomitantly (open green circle and filled blue circle). The kinematic sequence is completed as the body reaches its minimum speed and comes to a maximum pitch angle.



Williams et al., 2000), given that complete lunge collapse is suggested to occur at a depth of about 100 m (Scholander, 1940; Ridgway et al., 1969; Ridgway and Howard, 1979). Williams et al. also observed gait transition at similar depths for the blue whale, *Balaenoptera musculus* (Williams et al., 2000). Negative buoyancy may be counteracted by hydrodynamic lift provided by the pectoral flippers as they are abducted and extended away from the body (Fish and Battle, 1995; Miklosovich et al., 2004). Accordingly, tethered minke and sei whales were observed to sink while the flippers were held against the body and pitch toward the surface when they were extended (Williamson, 1972). *Balaenoptera* are also reported to be negatively buoyant and typically sink when killed (Slijper, 1962; Brodie, 1977).

In order to utilize oxygen stores wisely at depth, diving animals must not only reduce locomotor activity but also exhibit an efficient mode of locomotion. The morphological design of the fin whale is well equipped for efficient, high-speed swimming (Bose and Lien, 1989; Bose et al., 1990). Fin whales are theoretically capable of speeds as high as 13 m s^{-1} (Bose and Lien, 1989), and maximum speeds of up to 10 m s^{-1} have been reported (Gambell, 1985). Average speeds observed over long-distance tracks, however, are only $0.5\text{--}2.0 \text{ m s}^{-1}$ (Notarbartolo-di-Sciara et al., 2003). In the present study,

sustained speeds during ascent (Table 1) were within the range predicted to be efficient ($2\text{--}10 \text{ m s}^{-1}$) but were quite lower than those predicted to produce maximum propulsive efficiency ($6\text{--}8 \text{ m s}^{-1}$) by unsteady hydrofoil theory (Bose and Lien, 1989). Maximum speeds estimated for fin whales on descent ($5.7 \pm 0.3 \text{ m s}^{-1}$; Table 1) were significantly lower than maximum swim speeds observed in both captive and wild delphinids (Rohr et al., 2002). With respect to body size, the speeds observed in this study by fin whales are very low in comparison with odontocetes.

The kinematics of the body and flukes during lunges depict an exceptionally dynamic event. Body acceleration driven by a bout of fluking is immediately met by a relatively larger deceleration, probably due to the opening of the mouth. Lowering of the mandibles increases the surface area of the body, specifically the buccal cavity, perpendicular to flow. The moving buccal cavity meeting the stationary volume of prey-laden seawater provides the pressure needed to expand the ventral groove blubber in proportion to the square of velocity (Orton and Brodie, 1987). A large part of the kinetic energy of the body should be converted into potential energy stored in the stretched ventral groove blubber. The Y-shaped fibrocartilage skeleton that lies within the musculature of the ventral pouch may provide structural rigidity to the region or

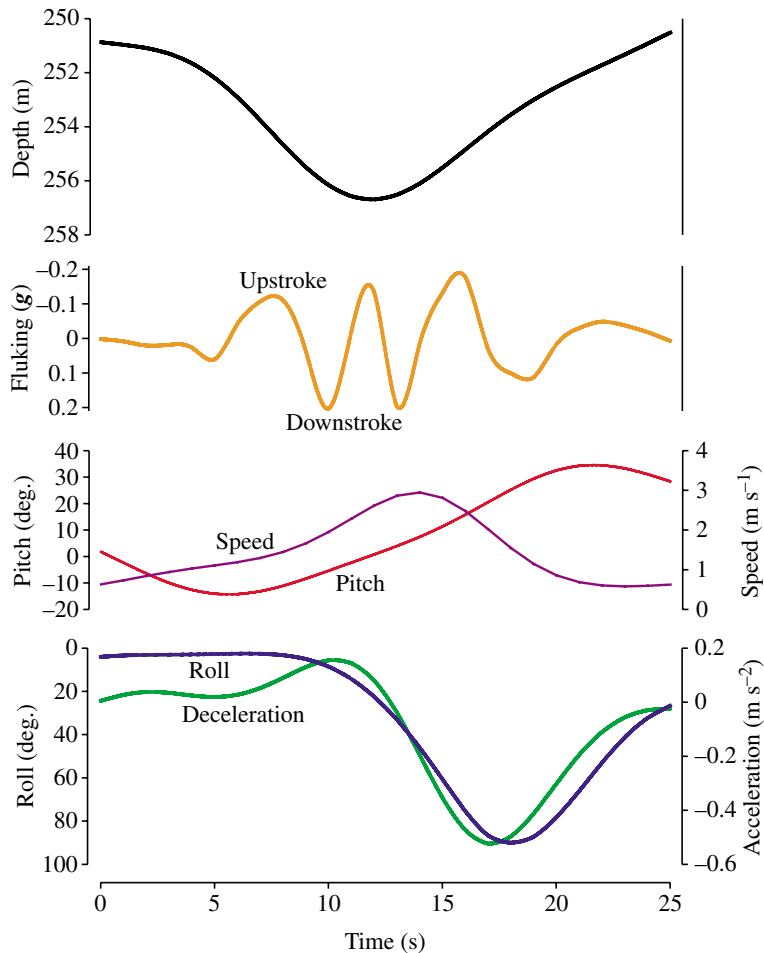


Fig. 10. Body and fluke mechanics during one lateral lunge. Kinematic parameters follow the definitions from Fig. 9. Note the temporal coordination between body roll and body deceleration.

act as a tendon to distribute forces involved in the feeding process (Pivorunas, 1977). Once the buccal cavity is filled, the 'elongated, bloated tadpole' profile of the body (Orton and Brodie, 1987) must also increase drag on the body and contribute to the overall deceleration of the body.

Accelerating a large body is energetically demanding. This appears to be the reason why lunge-feeding is so costly and thus limits dive time. Since drag on the body is proportional to the square of its instantaneous velocity, the thrust and energy needed to overcome drag will be high during a lunge. In addition, drag should become dramatically larger when the mouth is agape, dissipating the kinetic energy of the body. Our data support the hypothesis by Acevedo-Gutierrez et al. that the rapid changes in speed associated with lunge-feeding at depth are energetically expensive and limit dive capacity in rorqual whales (Acevedo-Gutierrez et al., 2002). Quite the opposite seems to be the case for bowhead and right whales, which appear to swim at relatively constant speeds (Nowacek et al., 2001) and continuously filter feed *via* both hydrodynamic and ram hydraulic pressures (Werth, 2004; Lambertsen et al., 2005). According to mechanical principles,

this foraging strategy should be energetically more efficient than lunge-feeding since the body maintains a relatively constant speed and thus accelerations of the center of mass will be minimized. Bowhead whale dive behavior is consistent with this hypothesis; they exhibit longer dive durations and shorter recovery times between dives than a larger blue whale diving to the same depth (Dorsey et al., 1989; Würsig and Clark, 1993; Krutzikowsky and Mate, 2000; Croll et al., 2001).

Steady fluking that occurs during the ascent phase of a dive must also come at an energetic cost since the whale is negatively buoyant, but this should not be as costly as lunging given that speed on ascent remained relatively constant (Fig. 6). Therefore, it is not surprising to observe rorquals performing deep dives of limited duration (Panigada et al., 1999), as long as the number of lunges per dive is low. Body acceleration observed over the course of ascent decreases steadily (Fig. 8B), perhaps indicating fatigue. However, it may also indicate a decrease in motivation associated with gradually changing buoyant forces near the end of ascent. From these kinematic data it is unclear whether fin whales were exceeding their aerobic capacity during foraging dives.

The maximum speeds recorded at jaw opening match the predictions made by Orton and Brodie for the hydrodynamic forces needed to expand the ventral groove blubber if feeding was exclusively powered by the locomotor muscles (Orton and Brodie, 1987). Also, the slight downward pitch of the body just prior to the lunge may help to open the mouth by lowering the pressure on the underside of the head *via* the Bernoulli effect. Our results show that fin whales fluke throughout each lunge (Figs 9, 10), even after jaw opening, supporting the hypothesis that prey-laden water is enveloped by the buccal cavity (Orton and Brodie, 1987). The timing of jaw opening is critical for successful prey capture in order to avoid pushing prey away with a bow wave (Brodie, 1977) and is likely facilitated by the tactile sensing of prey *via* vibrissae on the mandibles (Ogawa and Shida, 1950; Gaskin, 1982). Contraction of the buccal cavity must occur when the whale is gliding between lunges. If we assume that engulfment is accomplished in the time elapsed during a fluking bout (16.2 ± 3.9 s; Table 2) and that a fin whale engulfs approximately 30 m^3 of water and prey during a lunge (see a previous estimate of 70 m^3 for a blue whale) (Pivorunas, 1979), water must be filtered at a rate of nearly $1 \text{ m}^3 \text{ s}^{-1}$, since durations between each consecutive lunge were 44.5 ± 19.1 s. However, we do not know the extent to which the buccal cavities were filled during each lunge, as there have been previous accounts of fin and sei whales engulfing prey without the buccal cavity becoming 'enormously expanded' (Pivorunas, 1979). In addition, estimates for the volume of engulfed prey and water are entirely anecdotal.

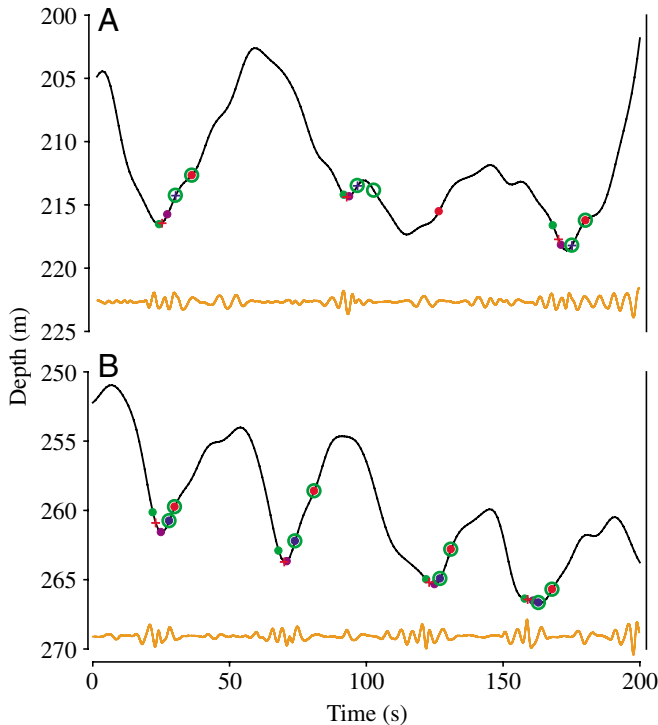


Fig. 11. Two kinematic modes observed during lunges. Kinematics of the body and fluke are largely conserved among all individuals for both regular lunges (A) and lateral lunges (B). Maxima, minima and zero values for kinematic parameters follow the definitions from Fig. 9. Note that for regular lunges the body is not rolled, but level as the body experiences its greatest deceleration.

Lunges occurred in two distinct modes, which were distinguished by the degree of body roll at the moment of jaw opening (Figs 9, 10). Lateral lunges involved a 90° roll to the same side on each lunge, while regular lunges involved no significant roll as the body reached maximum velocity. Why *Balaenoptera* roll during lunges is not known. Rotating about the longitudinal axis may orient the jaws in such a way as to capture prey by anticipating their escape trajectory (F. E. Fish, personal communication). Lateral lunges may also be a way to pin or drive prey against a barrier, such as the sea surface or sea floor. Being negatively buoyant, a 90° roll may help with maneuvers in the plane perpendicular to buoyancy, where they are weight neutral (B. Ahlborn, personal communication). Both behaviors have been previously observed among the rorquals (Andrews, 1909; Tomilin, 1957; Jurasz and Jurasz, 1979; Watkins and Schevill, 1979; Gaskin, 1982; Hain et al., 1995; Corkeron, 1999). Gaskin, who reported both lateral and regular lunges for fin whales off the southwestern coast of Nova Scotia (Gaskin, 1982), suggested that regular lunges were generally less effective and mainly directed towards fish rather than euphausiids.

Cetacean maneuvers are primarily driven by lift derived from the flukes and by the asymmetrical orientation and/or movement of the flippers (Edel and Winn, 1978; Fish, 2002; Fish, 2004; Fish et al., 2006). Our data show that body rotation,

particularly roll, occurs during fluking bouts associated with lunges (Fig. 9). However, rolling was sometimes observed during glides, especially in individuals that exhibited regular lunges, suggesting that fin whales employ both powered and non-powered lift-based mechanisms to maneuver. Edel and Winn reported flipper movement and twisting of the caudal stock and fluke during banked turns in the humpback whale (Edel and Winn, 1978). Fin whales performing lateral lunges at the sea surface exhibited strong fluking in coordination with lateral extensions of a pivotal flipper (Gaskin, 1982). We were not able to discern flipper movement during lunges, so the extent to which torque generated by the fluke was enhanced by control surfaces remains undetermined for fin whales.

Although three-dimensional dive behavior has been described for phocid seals (Davis et al., 2001; Davis et al., 2003; Mitani et al., 2003; Mitani et al., 2004), comprehensive data showing maneuvers effected by six kinematic degrees of freedom have not been presented for any marine mammal. Our analysis was only able to resolve two kinematic degrees of freedom with respect to body rotation, so changes in yaw that occurred through the dive cycle were not unknown. As a result, the roll moments recorded could have been associated with maneuvering, as has been observed for beaked whales maneuvering to capture prey (Madsen et al., 2005). Considering the repeatable and modal nature of the behaviors observed (Fig. 8), we suspect that fin whales were spinning about their longitudinal axis, executing lateral lunges similar to what was qualitatively described for humpback whales at the sea surface (Jurasz and Jurasz, 1979) and along the sea floor (Hain et al., 1995). However, lateral lunge-feeding behavior can involve a curvilinear trajectory (Gaskin, 1982). During regular lunges, roll moments were often observed just before maximum velocity, perhaps indicating a maneuver or banked turn towards a prey patch. These types of complex maneuvers typically involve temporal coupling of yaw and roll moments in flying animals (Schilstra and Van Hateren, 1999; Horisawa et al., 2003). More tagging efforts are necessary in order to determine body yaw and thus resolve full three-dimensional dive behavior in the context of local bathymetry and prey distribution (Mitani et al., 2003; Mitani et al., 2004; Watanabe et al., 2003).

We especially thank Bill Burgess at Greeneridge Sciences, Inc. for building an excellent, high-resolution Bioacoustic Probe. We also thank Bill Burgess, Frank Fish, Robert Dudley, Jerry Kooyman, Torre Knowler, Megan McKenna, Jessica Meir, Paul Murphy, Nick Pyenson, Melissa Soldevilla and Greg Szulgit for providing useful comments on the manuscript. We thank Sean Wiggins for assistance with visualizing local sea floor bathymetry. Funding was provided by the United States Navy (SERDP Robert Holst, CNO-N45 Frank Stone, ONR Bob Gisiner) and NSERC to R.E.S.

References

- Acevedo-Gutierrez, A., Croll, D. A. and Tershy, B. R. (2002). High feeding costs limit dive time in the largest whales. *J. Exp. Biol.* **205**, 1747-1753.

- Andrews, R. C. (1909). Observations on the habits of the finback and humpback whales of the eastern North Pacific. *Bull. Am. Mus. Nat. Hist.* **26**, 213-216.
- Arnold, P. W., Birtles, R. A., Sobotzick, S., Matthews, M. and Dunstan, A. (2005). Gulping behaviour in rorqual whales: underwater observations and functional interpretation. *Mem. Queensl. Mus.* **51**, 309-332.
- Bigelow, H. B. and Schroeder, W. C. (1953). Fishes in the Gulf of Maine. *US Fish Wild. Serv. Fish. Bull.* **53**, 1-577.
- Bose, N. and Lien, J. (1989). Propulsion of a fin whale (*Balaenoptera physalus*): why the fin whale is a fast swimmer. *Proc. R. Soc. Lond. B Biol. Sci.* **237**, 175-200.
- Bose, N., Lien, J. and Ahia, J. (1990). Measurements of the bodies and flukes of several cetacean species. *Proc. R. Soc. Lond. B Biol. Sci.* **242**, 163-173.
- Brodie, P. F. (1975). Cetacean energetics, an overview of intraspecific size variation. *Ecology* **56**, 152-161.
- Brodie, P. F. (1977). Form, function and energetics of cetacea: a discussion. In *Functional Anatomy of Marine Mammals*, vol. 3 (ed. R. J. Harrison), pp. 45-56. New York: Academic Press.
- Brodie, P. F. (1993). Noise generated by the jaw actions of feeding fin whales. *Can. J. Zool.* **71**, 2546-2550.
- Burgess, W. C., Tyack, P. L., Le Boeuf, B. J. and Costa, D. P. (1998). A programmable acoustic recording tag and first results from free-ranging northern elephant seals. *Deep-Sea Res. II Top. Stud. Oceanogr.* **45**, 1327-1351.
- Butler, P. J. and Jones, D. R. (1982). The comparative physiology of diving. *Adv. Comp. Physiol. Biochem.* **8**, 179-364.
- Butler, P. J. and Jones, D. R. (1997). Physiology of diving of birds and mammals. *Physiol. Rev.* **77**, 837-899.
- Calder, W. A. (1984). *Size, Function, and Life History*. Cambridge, MA: Harvard University Press.
- Castellini, M. A., Murphy, B. J., Fedak, M., Ronald, K., Gofton, N. and Hochachka, P. W. (1985). Potentially conflicting metabolic demands of diving and exercise in seals. *J. Appl. Physiol.* **58**, 392-399.
- Corkeron, P. J., Ensor, P. and Matsuoka, K. (1999). Observations of blue whales feeding in Antarctic waters. *Polar Biol.* **22**, 213-215.
- Croll, D. A., Tershy, B. R., Hewitt, R. P., Demer, D. A., Fiedler, P. C., Smith, S. E., Armstrong, W., Popp, J. M., Kiekhefer, T., Lopez, V. R. et al. (1998). An integrated approach to the foraging ecology of marine birds and mammals. *Deep-Sea Res. II Top. Stud. Oceanogr.* **45**, 1353-1371.
- Croll, D. A., Acevedo-Gutierrez, A., Tershy, B. R. and Urban-Ramirez, J. (2001). The diving behavior of blue and fin whales: is dive duration shorter than expected based on oxygen stores? *Comp. Biochem. Physiol.* **129A**, 797-809.
- Croll, D. A., Marinovic, B., Benson, S., Chavez, F. P., Black, N., Ternullo, R. and Tershy, B. R. (2005). From wind to whales: trophic links in a coastal upwelling system. *Mar. Ecol. Prog. Ser.* **289**, 117-130.
- Davis, R. W., Williams, T. M. and Kooyman, G. L. (1985). Swimming metabolism of yearling and adult harbor seals *Phoca-vitulina*. *Physiol. Zool.* **58**, 590-596.
- Davis, R. W., Fuiman, L. A., Williams, T. M. and Le Boeuf, B. J. (2001). Three-dimensional movements and swimming activity of a northern elephant seal. *Comp. Biochem. Physiol.* **129A**, 759-770.
- Davis, R. W., Fuiman, L. A., Williams, T. M., Horning, M. and Hagey, W. (2003). Classification of Weddell seal dives based on 3-dimensional movements and video-recorded observations. *Mar. Ecol. Prog. Ser.* **264**, 109-122.
- Davis, R. W., Polasek, L., Watson, R., Fuson, A., Williams, T. M. and Kanatous, S. B. (2004). The diving paradox: new insights into the role of the dive response in air-breathing vertebrates. *Comp. Biochem. Physiol.* **138A**, 263-268.
- deBakker, M. A. G., Kastelein, R. A. and Dubbeldam, J. L. (1997). Histology of the grooved ventral pouch of the minke whale, *Balaenoptera acutorostrata*, with special reference to the occurrence of lamellated corpuscles. *Can. J. Zool.* **75**, 563-567.
- Dorsey, E. M., Richardson, W. J. and Würsig, B. (1989). Factors affecting surfacing, respiration and dive behaviour of bowhead whales, *Balaena mysticetus*, summering in the Beaufort Sea. *Can. J. Zool.* **67**, 1801-1815.
- Edel, R. K. and Winn, H. E. (1978). Observations on underwater locomotion and flipper movement of the humpback whale *Megaptera novaeangliae*. *Mar. Biol.* **48**, 279-287.
- Fiedler, P. C., Reilly, S. B., Hewitt, R. P., Demer, D., Philbrick, V. A., Smith, S., Armstrong, W., Croll, D. A., Tershy, B. R. and Mate, B. R. (1998). Blue whale habitat and prey in the California Channel Islands. *Deep Sea Res. II Top. Stud. Oceanogr.* **45**, 1781-1801.
- Finger, R. A., Abbagnaro, L. A. and Bauer, B. B. (1979). Measurements of low-velocity flow noise on pressure and pressure-gradient hydrophones. *J. Acoust. Soc. Am.* **65**, 1407-1412.
- Fish, F. E. (1993a). Influence of hydrodynamic design and propulsive mode on mammalian energetics. *Aust. J. Zool.* **42**, 79-101.
- Fish, F. E. (1993b). Power output and propulsive efficiency of swimming bottlenose dolphins (*Tursiops truncatus*). *J. Exp. Biol.* **185**, 179-193.
- Fish, F. E. (1998). Comparative kinematics and hydrodynamics of odontocete cetaceans: morphological and ecological correlates with swimming performance. *J. Exp. Biol.* **201**, 2867-2877.
- Fish, F. E. (2002). Balancing requirements for stability and maneuverability in cetaceans. *Integr. Comp. Biol.* **42**, 85-93.
- Fish, F. E. (2004). Structure and mechanics of nonpiscine control surfaces. *IEEE J. Ocean. Eng.* **29**, 605-621.
- Fish, F. E. and Battle, J. M. (1995). Hydrodynamic design of the humpback whale flipper. *J. Morphol.* **225**, 51-60.
- Fish, F. E. and Rohr, J. (1999). Review of dolphin hydrodynamics and swimming performance. In *SPAWARS System Center Technical Report 1801*. San Diego, CA.
- Fish, F. E., Innes, S. and Ronald, K. (1988). Kinematics and estimated thrust production of swimming harp and ringed seals. *J. Exp. Biol.* **137**, 157-173.
- Fish, F. E., Peacock, J. E. and Rohr, J. J. (2003). Stabilization mechanism in swimming odontocete cetaceans by phased movements. *Mar. Mamm. Sci.* **19**, 515-528.
- Fish, F. E., Nicastro, A. J. and Weihs, D. (2006). Dynamics of the aerial maneuvers of spinner dolphins. *J. Exp. Biol.* **209**, 590-598.
- Fletcher, S., Le Boeuf, B. J., Costa, D. P., Tyack, P. L. and Blackwell, S. B. (1996). Onboard acoustic recording from diving northern elephant seals. *J. Acoust. Soc. Am.* **100**, 2531-2539.
- Gambell, R. (1985). Finwhale *Balaenoptera physalus*. In *Handbook of Marine Mammals* (ed. S. H. Ridgeway and R. J. Harrison), pp. 3171-3192. Toronto, ON: Academic Press.
- Gaskin, D. E. (1982). *The Ecology of Whales and Dolphins*. London: Heinemann.
- Hain, J. H. W., Ellis, S. L., Kenney, R. D., Clapham, P. J., Gray, B. K., Weinrich, M. T. and Babb, I. G. (1995). Apparent bottom feeding by humpback whales on Stellwagen Bank. *Mar. Mamm. Sci.* **11**, 464-479.
- Halsey, L. G., Butler, P. J. and Blackburn, T. M. (2006). A phylogenetic analysis of the allometry of diving. *Am. Nat.* **167**, 276-287.
- Hochachka, P. W. (1986). Balancing conflicting metabolic demands of exercise and diving. *Fed. Proc.* **45**, 2948-2952.
- Horisawa, S., Byrnes, G., Goldbogen, J. A., Clark, C. and Dudley, R. (2003). Three-dimensional flight maneuvers in hummingbirds. *Second International Symposium on Aqua Bio-Mechanisms*. Honolulu, Hawaii.
- Jurasz, C. M. and Jurasz, V. P. (1979). Feeding modes of the humpback whale, *Megaptera novaeangliae*, in southeast Alaska. *Sci. Rep. Whales Res. Inst.* **31**, 69-83.
- Kleiber, M. (1932). Body size and metabolism. *Hilgardia* **6**, 315-353.
- Kot, B. W. (2005). Rorqual whale surface-feeding strategies: biomechanical aspects of feeding anatomy and exploitation of prey aggregations along tidal fronts. M.Sc. thesis, University of California, Los Angeles.
- Kooyman, G. L. (1989). *Diverse Divers*. Berlin: Springer-Verlag.
- Kooyman, G. L. and Ponganis, P. J. (1998). The physiological basis of diving to depth: birds and mammals. *Annu. Rev. Physiol.* **60**, 19-32.
- Krutzkowsky, G. K. and Mate, B. R. (2000). Dive and surface characteristics of bowhead whales (*Balaena mysticetus*) in the Beaufort and Chukchi seas. *Can. J. Zool.* **78**, 1182-1198.
- Lambertsen, R. H. (1983). Internal mechanism of rorqual feeding. *J. Mammal.* **64**, 76-88.
- Lambertsen, R. H. and Hintz, R. J. (2004). Maxillomandibular cam articulation discovered in north Atlantic minke whale. *J. Mammal.* **85**, 446-452.
- Lambertsen, R., Ulrich, N. and Straley, J. (1995). Frontomandibular stay of balaenopteridae – a mechanism for momentum recapture during feeding. *J. Mammal.* **76**, 877-899.
- Lambertsen, R. H., Rasmussen, K. J., Lancaster, W. C. and Hintz, R. J. (2005). Functional morphology of the mouth of the bowhead whale and its implications for conservation. *J. Mammal.* **86**, 342-352.
- Madsen, P. T., Johnson, M., Aguilar de Soto, N., Zimmer, W. M. X. and Tyack, P. (2005). Biosonar performance of foraging beaked whales (*Mesoplodon densirostris*). *J. Exp. Biol.* **208**, 181-194.
- Miklosovic, D. S., Murray, M. M., Howle, L. E. and Fish, F. E. (2004). Leading-edge tubercles delay stall on humpback whale (*Megaptera novaeangliae*) flippers. *Phys. Fluids* **16**, L39-L42.

- Miller, P. J. O., Johnson, M. P., Tyack, P. L. and Terray, E. A.** (2004). Swimming gaits, passive drag and buoyancy of diving sperm whales *Physeter macrocephalus*. *J. Exp. Biol.* **207**, 1953-1967.
- Mitani, Y., Sato, K., Ito, S., Cameron, M. F., Siniff, D. B. and Naito, Y.** (2003). A method for reconstructing three-dimensional dive profiles of marine mammals using geomagnetic intensity data: results from two lactating Weddell seals. *Polar Biol.* **26**, 311-317.
- Mitani, Y., Watanabe, Y., Sato, K., Cameron, M. F. and Naito, Y.** (2004). 3D diving behavior of Weddell seals with respect to prey accessibility and abundance. *Mar. Ecol. Prog. Ser.* **281**, 275-281.
- Noren, S. R. and Williams, T. M.** (2000). Body size and skeletal muscle myoglobin of cetaceans: adaptations for maximizing dive duration. *Comp. Biochem. Physiol.* **126A**, 181-191.
- Notarbartolo-di-Sciara, G., Zanardelli, M., Jahoda, M., Panigada, S. and Airoldi, S.** (2003). The fin whale *Balaenoptera physalus* (L 1758) in the Mediterranean Sea. *Mammal Rev.* **33**, 105-150.
- Nottestad, L., Ferno, A., Mackinson, S., Pitcher, T. and Misund, O. A.** (2002). How whales influence herring school dynamics in a cold-front area of the Norwegian Sea. *ICES J. Mar. Sci.* **59**, 393-400.
- Nowacek, D. P., Johnson, M. P., Tyack, P. L., Shorter, K. A., McLellan, W. A. and Pabst, D. A.** (2001). Buoyant balaenids: the ups and downs of buoyancy in right whales. *Proc. R. Soc. Lond. B Biol. Sci.* **268**, 1811-1816.
- Ogawa, T. and Shida, T.** (1950). On the sensory tubercles of lips and oral cavity in the sei and fin whale. *Sci. Rep. Whales Res. Inst.* **3**, 1-16.
- Oleson, E. M.** (2005). Calling behavior of blue and fin whales off California. Ph.D. thesis, University of California, San Diego.
- Orton, L. S. and Brodie, P. F.** (1987). Engulfing mechanics of fin whales. *Can. J. Zool.* **65**, 2898-2907.
- Overholtz, W. J. and Nicolas, J. R.** (1979). Apparent feeding by the fin whale, *Balaenoptera physalus*, and humpback whale, *Megaptera novaengliae*, on the American sand lance, *Ammodytes americanus*, in the Northwest Atlantic. *Fish. Bull.* **77**, 285-287.
- Panigada, S., Zanardelli, M., Canese, S. and Jahoda, M.** (1999). How deep can baleen whales dive? *Mar. Ecol. Prog. Ser.* **187**, 309-311.
- Pivorunas, A.** (1977). Fibrocartilage skeleton and related structures of ventral pouch of balaenopterid whales. *J. Morphol.* **151**, 299-313.
- Pivorunas, A.** (1979). Feeding mechanisms of baleen whales. *Am. Sci.* **67**, 432-440.
- Rice, D. W.** (1998). *Marine Mammals of the World: Systematics and Distribution. Special Publication Number 4*. Lawrence, KS: The Society of Marine Mammalogy.
- Ridgway, S. H. and Howard, R.** (1979). Dolphin lunge collapse and intramuscular circulation during free diving: Evidence from nitrogen washout. *Science* **206**, 1182-1183.
- Ridgway, S. H., Scronce, B. L. and Kanwisher, J.** (1969). Respiration and deep diving in the bottlenose porpoise. *Science* **166**, 1651-1654.
- Rohr, J. J., Fish, F. E. and Gilpatrick, J. W.** (2002). Maximum swim speeds of captive and free-ranging delphinids: critical analysis of extraordinary performance. *Mar. Mamm. Sci.* **18**, 1-19.
- Sato, K., Mitani, Y., Cameron, M. F., Siniff, D. B. and Naito, Y.** (2003). Factors affecting stroking patterns and body angle in diving Weddell seals under natural conditions. *J. Exp. Biol.* **206**, 1461-1470.
- Schilstra, C. and Van Hateren, J. H.** (1999). Blowfly flight and optic flow. I. Thorax kinematics and flight dynamics. *J. Exp. Biol.* **202**, 1481-1490.
- Scholander, P. F.** (1940). Experimental investigations on the respiratory function in diving mammals and birds. *Hvalradets Skrifter* **22**, 1-131.
- Schreer, J. F. and Kovacs, K. M.** (1997). Allometry of diving capacity in air-breathing vertebrates. *Can. J. Zool.* **75**, 339-358.
- Simard, Y., Lavoie, D. and Saucier, F. J.** (2002). Channel head dynamics: capelin (*Mallotus villosus*) aggregation in the tidally driven upwelling system of the Saguenay St. Lawrence Marine Park's whale feeding ground. *Can. J. Fish. Aquat. Sci.* **59**, 197-210.
- Skrovan, R. C., Williams, T. M., Berry, P. S., Moore, P. W. and Davis, R. W.** (1999). The diving physiology of bottlenose dolphins (*Tursiops truncatus*) – II. Biomechanics and changes in buoyancy at depth. *J. Exp. Biol.* **202**, 2749-2761.
- Slijper, E. J.** (1962). *Whales*. London: Hutchinson.
- Snyder, G. K.** (1983). Respiratory adaptations in diving mammals. *Respir. Physiol.* **54**, 269-294.
- Tomilin, A. G.** (1957). *The Mammals of the USSR and Adjacent Countries, Vol. IX, Cetacea*. Moscow: Izdatel'stvo Akademi Nauk SSR.
- Vogel, S.** (1994). *Life in Moving Fluids: The Physical Biology of Flow* (2nd edn). Princeton, NJ: Princeton University Press.
- Watanabe, Y., Mitani, Y., Sato, K., Cameron, M. F. and Naito, Y.** (2003). Dive depths of Weddell seals in relation to vertical prey distribution as estimated by image data. *Mar. Ecol. Prog. Ser.* **252**, 283-288.
- Watkins, W. A. and Schevill, W. E.** (1979). Aerial observation of feeding behavior in 4 baleen whales: *Eubalaena glacialis*, *Balaenoptera borealis*, *Megaptera novaengliae*, and *Balaenoptera physalus*. *J. Mammal.* **60**, 155-163.
- Webb, P. W. and de Buffrenil, V.** (1990). Locomotion in the biology of large aquatic vertebrates. *Trans. Am. Fish. Soc.* **119**, 629-641.
- Weih, D.** (1981). Effect of swimming path curvature on the energetics of fish. *Fish. Bull.* **79**, 171-176.
- Weih, D. and Webb, P. W.** (1983). Optimization of locomotion. In *Fish Biomechanics* (ed. P. W. Webb and D. Weih), pp. 339-371. New York: Praeger.
- Werth, A. J.** (2000). Feeding in marine mammals. In *Feeding: Form, Function and Evolution in Tetrapod Vertebrates* (ed. K. Schwenk), pp. 475-514. New York: Academic Press.
- Werth, A. J.** (2004). Models of hydrodynamic flow in the bowhead whale filter feeding apparatus. *J. Exp. Biol.* **207**, 3569-3580.
- Williams, T. M.** (2001). Intermittent swimming by mammals: a strategy for increasing energetic efficiency during diving. *Am. Zool.* **41**, 166-176.
- Williams, T. M., Davis, R. W., Fuiman, L. A., Francis, J., Le Boeuf, B. L., Horning, M., Calambokidis, J. and Croll, D. A.** (2000). Sink or swim: strategies for cost-efficient diving by marine mammals. *Science* **288**, 133-136.
- Williams, T. M., Fuiman, L. A., Horning, M. and Davis, R. W.** (2004). The cost of foraging by a marine predator, the Weddell seal *Leptonychotes weddellii*: pricing by the stroke. *J. Exp. Biol.* **207**, 973-982.
- Williamson, G. R.** (1972). The true body shape of rorqual whales. *J. Zool. Lond.* **167**, 277-286.
- Würsig, B. and Clark, C. W.** (1993). Behavior. In *The Bowhead Whale* (ed. J. H. Burns, J. J. Montague and C. J. Cowles), pp. 157-199. Lawrence, KS: Allen Press.